Modeling of a novel InP-based monolithically integrated magneto-optical waveguide isolator

K. Postava

Department of Physics, Technical University of Ostrava, 17 listopadu 15, 708 33 Ostrava-Poruba, Czech Republic

M. Vanwolleghem, D. Van Thourhout, and R. Baets

Department of Information Technology, Ghent University, Interuniversitair Micro-Electronica Centrum, St-Pietersnieuwstraat 41, 9000 Ghent, Belgium

Š. Višňovský

Institute of Physics, Charles University of Prague, Ke Karlovu 5, 121 16 Prague 2, Czech Republic

P. Beauvillain

Institut d'Electronique Fondamentale, Unité Mixte de Recherche Centre National de la Recherche Scientifique 8622, Université Paris-Sud, Orsay, France

J. Pištora

Department of Physics, Technical University of Ostrava, 17 listopadu 15, 708 33 Ostrava-Poruba, Czech Republic

Received June 7, 2004; accepted August 2, 2004; revised manuscript received September 16, 2004

A method based on Yeh's rigorous 4 × 4 matrix algebra and a fast perturbation-theory-based method are proposed for modeling and optimization of an integrated magneto-optical (MO) waveguide isolator. The transverse MO Kerr effect in ferromagnetic $Co_{90}Fe_{10}$ is used to design the integrated isolator. Waveguide losses introduced by absorption in the MO metallic film are compensated for by optical gain in an InP-based semiconductor optical amplifier with a tensile strained multiple-quantum-well (MQW) active region. The desired device isolation, which originates from the nonreciprocity of the transverse MO effect, is obtained by operation of the device under appropriate current injection, leading to zero modal net gain in the forward direction while the device remains lossy in the backward direction. In the approach based on Yeh's matrix formalism, phenomena such as the MO effects described by anisotropic permittivity tensors, waveguide losses in absorbing layers, and optical gain in the active layer are explicitly included. Numerical aspects of the resonant condition solution for waveguide modes are discussed. In the perturbation theory method, the MO nonreciprocal waveguide effects are calculated in a first-order scheme. The general models are applied in an example of a realistic InP-based MQW isolator with a $Co_{90}Fe_{10}$ MO layer, indicating that practical isolation ratios are achievable within reasonable levels of necessary material gain. Rigorous and perturbation models are compared, and good agreement is obtained. This result indicates that first-order perturbation theory modeling of integrated magneto-optics is accurate enough, even for devices that employ MO materials with relatively strong Voigt parameters.

OCIS codes: 230.3240, 230.3810, 130.3120.

1. INTRODUCTION

To ensure stable emission of a semiconductor laser, an optical isolator is needed to prevent undesirable backreflections. The nonreciprocity of magneto-optical (MO) effects becomes a basis of such devices. Despite the fact that traditional free-space bulk isolators are cheap and compact devices with strong isolation ratios up to 60 dB, expensive submicrometer alignment techniques are needed to incorporate these components into the laser package. This requirement has an effect on the total cost of a commercial laser diode. Moreover, the integration of a big diversity of optical functions on a single chip, as is expected to occur in future photonic integrated circuits for all-optical signal processing, underlines the need for an integrated optical isolator. Integration also increases the thermal and mechanical stability of the device, requires a smaller saturation magnetic field, and permits a high level of integration with low insertion loss.

The development of an integrated optical waveguide isolator has therefore been a subject of intense research for the past decades.[1–6] Several designs have been successfully experimentally demonstrated. Stand-alone waveguide isolator devices have been reported with isolation ratios up to 30 dB.[7,8] However, the majority of integrated isolator designs have been based on the same materials as those used in their bulk free-space counterparts, i.e., rare-earth ferrimagnetic iron garnets ($RE_3Fe_5O_{12}$). These materials are transparent and show sufficiently strong Faraday rotation in the wavelength range of optical telecommunication. However, the integration of this garnet system with traditional III–V semiconductor substrates has faced great technological diffi-

0740-3224/2005/010261-13$15.00

culties. The most popular technique encountered nowadays to integrate these garnet-based materials with InP substrates makes use of direct bonding of wafers.[9,10]

A completely novel approach to integration of optical nonreciprocity in a semiconductor photonic integrated circuit was theoretically suggested a few years ago.[11,12] The approach is based on inducing the transverse magneto-optic Kerr effect[13] in a standard InP-based semiconductor optical amplifier (SOA) by replacing the traditional Au-based electric metal contact with a transversely magnetized MO metal contact, which will result in a nonreciprocal gain–loss behavior for the TM modes of this active device. Unlike garnet-based integrated isolators, this integrated isolator can be directly monolithically integrated with standard active InP-based devices. Furthermore, ferromagnetic MO metals (such as CoFe alloys) can easily be sputter deposited onto III–V semiconductors. Therefore this device is a potential candidate for a cheap, tolerant, and easy to fabricate monolithically integrated optical isolator.

In this paper modeling and optimization of such a SOA isolator is discussed. In Section 2 the basic operation of the device is described. The key properties needed for successful experimental fabrication of the device are indicated. In Section 3 the theoretical background of the two modeling approaches is elaborated, and specific aspects of their numerical implementation are discussed. In Section 4 both methods are numerically compared by means of a hypothetical benchmark example and a realistic MO isolator structure.

2. NOVEL CONCEPT

The most popular designs for integrated MO waveguide isolators base their operation on a transverse MO nonreciprocal phase shift. Unlike the better-known MO Faraday rotation that is employed in traditional bulk free-space isolators, this effect does not induce nonreciprocal coupling between the two independent polarization states of the guided modes but rather introduces a nonreciprocal (or, in other words, a direction-dependent) correction to the propagation constant of the guided modes. A magnetization parallel to the layer interfaces and perpendicular to the direction of propagation of the light (transversal MO configuration) will induce a nonreciprocal phase shift in the TM (p-polarized) modes, whereas the propagation behavior of the TE (s-polarized) modes will remain reciprocal. It is important to note that there is no simple configuration of the magnetization that would permit a polarization-independent nonreciprocal phase shift.

If the MO material is lossless (as it is for iron garnets), this phase shift will be purely real. Counterpropagating TM modes will undergo an opposite phase change. It is obvious that one can exploit this effect to fabricate a nonreciprocal Mach–Zehnder interferometer, which would lead to constructive interference in the forward direction and to destructive interference in the backward direction. This principle is popular in garnet-based integrated waveguide isolators.[4–6,14] However, as was pointed out in Section 1, the experimental success of attempts at integrating these garnet-based integrated isolators with III–V semiconductor substrates has remained limited.[7] The main reason for this seems to be the technological difficulties posed by the wafer bonding techniques and the problems in achieving uniform magnetization of the garnet layers.[15]

A novel concept for integrating optical isolation in a photonic IC, as proposed by Takenaka and Nakano[11] and by Zaets and Ando,[12] is based on exploiting the imaginary part of the transverse MO Kerr effect for lossy MO materials. The best-known examples of such materials are the ferromagnetic transition metals and their alloys with nonnegligible real parts of the off-diagonal permittivity tensor elements. In the presence of transverse magnetization the effective extinction coefficients of a MO waveguide are different for forward and backward guided TM modes.[16] Isolation behavior is directly obtained by the difference in optical propagation loss of the forward and the backward modes. The magnitude of the phase shift is of course related to the amount of guided light that overlaps the lossy MO layer. Because there is easily an order-of-magnitude difference between the isotropic optical constants and the nonreciprocal MO constants of the various MO metals, it is clear that without additional loss compensation the device would be just an academic curiosity. Therefore the main idea of the novel concept is to combine the strong imaginary MO phase shift of ferromagnetic metals with a standard amplifying III–V semiconductor optical amplifier. In this way, one would achieve not only a way of compensating for the residual forward losses but at the same monolithic integration of optical nonreciprocity with InP-based active components. A schematic representation of the device is depicted in Fig. 1.

It is clear that experimental success for this device depends heavily on two important achievements: a high-quality ferromagnetic MO metal–semiconductor interface with acceptable optical, MO, magnetic, and electric properties, and a high-quality active semiconductor gain region. The former requirement is a consequence of the triple functionality that the MO metal needs to fulfill: It has at the same time to be a good ohmic contact for the underlying SOA, to be a good permanent magnet in the transverse direction (and thus to show sufficiently strong magnetic in-plane anisotropy), and to possess a strong MO constant in the optical telecom wavelength range of 1300–1600 nm. Successful experimental evidence that these requirements can be met was previously reported[17];

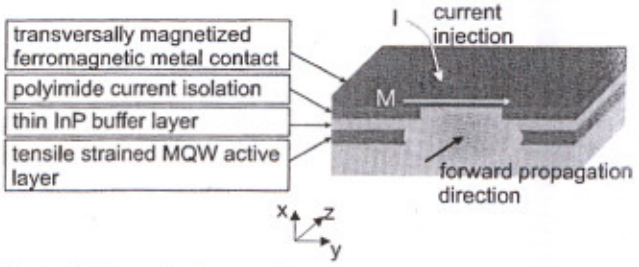

Fig. 1. Schematic of a two-dimensional cross section of a MO integrated isolator. A nonreciprocal gain shift originates from the transversal MO effect in a ferromagnetic metal film (M). Waveguide losses by the absorbing metal films are compensated for by optical gain in a MQW active region separated by an InP spacer layer. Both sides of the MO stripe waveguide are separated from the injection current by a polyimide isolating layer.

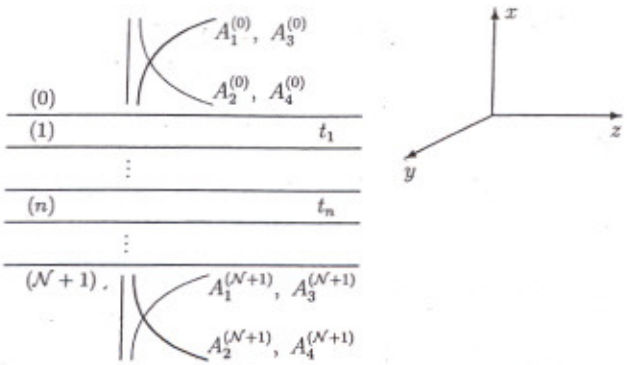

Fig. 2. Multilayer structure of the waveguide and the coordinate system chosen.

the ferromagnetic MO metal in those experiments was a sputter-deposited 50-nm thin film of $Co_{90}Fe_{10}$ alloy.

The need for a high-quality, high-gain active semiconductor region for compensation of forward loss requires optimized epitaxial growth of a tensile-strained multiple-quantum-well (MQW) layer. The need for tensile strain in the quantum wells (QWs) of the gain region is a direct consequence of the fact that a nonreciprocal MO transverse phase shift will influence only TM guided modes. TE waveguide modes will retain their reciprocal behavior. Therefore, unless the gain region of the underlying SOA structure provides strong gain discrimination between TE and TM polarization, any TE light that is present, which originated from spontaneous emission in the SOA or was generated by external sources, might undermine the operation of the device by adding noise to the output signal or even by saturating the gain performance of the MQW region. It is well known that one can tune the polarization selectivity of semiconductor gain by growing the QWs with a slight lattice mismatch and thus incorporating strain. Growing the QWs under tensile strain will lift the light-hole valence band above the heavy-hole valence band and thus favor TM light transitions in the active region.[18] Optimization of the epitaxial growth conditions has led to reports of a suitable tensile-strained MQW active region with TM modal gains that exceed 150 cm^{-1}.[19] The experimental successes described above have recently led to the experimental demonstration of an integrated isolator that incorporates this novel concept.[20,21]

3. THEORY

Waveguiding in a MO integrated isolator represents the problem of propagation of light in an anisotropic multilayer structure. In this paper a waveguide is represented as a system of $\mathcal{N}$ homogeneous layers separated by planar interfaces at $x = x_n$, $n = 0, 1, \ldots, \mathcal{N}$. The coordinate system is chosen as follows (see Fig. 2): the x axis is perpendicular to the interfaces, xz is the plane of incidence, and the z axis corresponds to the forward waveguiding direction. Note that this coordinate system is often used in integrated optics,[22] but it is different from that which is usually used in magneto-optics.[23] The field vectors are assumed to have $\exp(j\omega t)$ dependence, which corresponds to a monochromatic wave solution. The nth layer of thickness t_n is sandwiched between interface planes $x = x_{n-1}$ and $x = x_n$, $t_n = x_{n-1} - x_n$. The layer's medium is completely characterized by a relative permittivity tensor $\hat{\epsilon}^{(n)}$, whereas the magnetic permeability $\hat{\mu}^{(n)}$ is set to its vacuum value.

Boundary conditions for propagation of light in anisotropic multilayer structures are usually resolved by the compact matrix method.[24–26] In Subsection 3.A, Yeh's matrix algebra is elaborated for the general case of anisotropic multilayer waveguide structures. The general approach is then applied for transverse MO waveguides, i.e., those that contain layer(s) whose magnetization is perpendicular to the plane of incidence (direction of the y axis). Some specific aspects of transverse MO waveguides are discussed. For fast calculation and optimization, the MO isolation effects can be obtained from first-order perturbation theory as described in Subsection 3.B. The anisotropy that originates from MO effects is then regarded as a perturbation of the guided modes of the nonmagnetic waveguide. Advantages and disadvantages of both approaches are discussed in Subsection 3.C.

A. Rigorous Approach Based on Yeh's Matrix Algebra

Yeh's matrix algebra[23,25] represents a commonly used 4 × 4 matrix formalism for modeling of MO effects in multilayer structures. The calculation can be separated into three steps (see Fig. 3): (i) solving the wave equation in each anisotropic medium, thereby calculating the proper mode propagation vectors and the proper mode polarizations in each medium, (ii) formulating the boundary conditions in the form of a 4 × 4 matrix equation, resulting in a total multilayer stack transfer matrix **M**, and finally (iii) expressing the resonance condition for waveguide modes in terms of the total matrix elements M_{ij}.

1. Propagation of Light in a General Anisotropic Multilayer Structure

The field vectors can be assumed to have $\exp[j(\omega t - \mathbf{k}^{(n)}\mathbf{r})]$ dependence (i.e., to be plane monochromatic waves), where $\mathbf{k}^{(n)} = [k_x^{(n)} k_y k_z] = k_0[N_x^{(n)} N_y N_z]$ is the wave vector, $k_0 = \omega/c = 2\pi/\lambda$, and ω and λ denote the angular frequency and the wavelength, respectively. According to the coordinate system chosen, $N_y = 0$ and N_z represents the complex propagation constant often denoted n_{eff} in integrated optics. Because of Snell's law, the

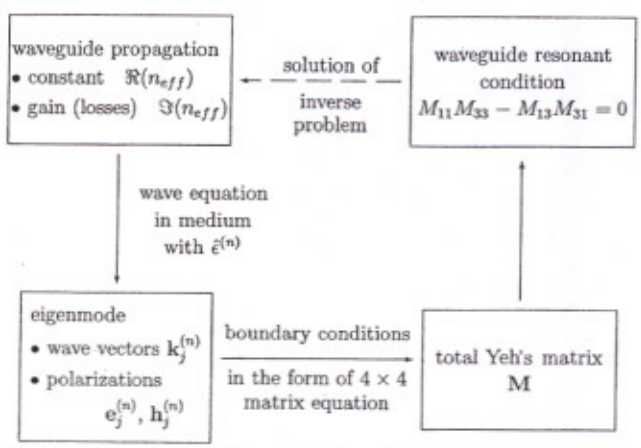

Fig. 3. Schematic of the application of Yeh's matrix algebra to produce the waveguide resonant condition and a solution of the inverse problem.

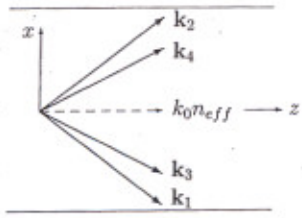

Fig. 4. Four eigenmodes propagating in an anisotropic layer.

tangential components of the wave vector, k_y and k_z (and also of N_y and $N_z \equiv n_{\text{eff}}$), are the same throughout the layered medium. In terms of the complex material tensors $\hat{\epsilon}^{(n)}$ and $\hat{\mu}^{(n)}$, Maxwell's equations for the nth medium become

$$\mathbf{k}^{(n)} \times \mathbf{H}_0{}^{(n)} = -\omega\epsilon_0\hat{\epsilon}^{(n)}\mathbf{E}_0{}^{(n)},$$
$$\mathbf{k}^{(n)} \times \mathbf{E}_0{}^{(n)} = \omega\mu_0\hat{\mu}^{(n)}\mathbf{H}_0{}^{(n)}, \tag{1}$$

where $\mathbf{E}_0$ and $\mathbf{H}_0$ denote the electric-field and the magnetic-field vectors, respectively. According to Eqs. (1), the wave equation can be obtained in the matrix form[27]

$$[\hat{\mathbf{N}}^{(n)}[\hat{\mu}^{(n)}]^{-1}\hat{\mathbf{N}}^{(n)} + \hat{\epsilon}^{(n)}]\mathbf{E}_0{}^{(n)} = \mathbf{0}, \tag{2}$$

where matrix $\hat{\mathbf{N}}$ is a vector product defined by

$$\mathbf{k}^{(n)} \times \mathbf{E}_0{}^{(n)} = k_0\hat{\mathbf{N}}^{(n)}\mathbf{E}_0{}^{(n)} = k_0\begin{bmatrix} 0 & -N_z & N_y \\ N_z & 0 & -N_x{}^{(n)} \\ -N_y & N_x{}^{(n)} & 0 \end{bmatrix}\mathbf{E}_0{}^{(n)}, \tag{3}$$

where $N_y = 0$ and $N_z \equiv n_{\text{eff}}$, corresponding to the coordinate system chosen. In Cartesian coordinates, wave Eq. (2) can be written in matrix form as

$$\begin{bmatrix} \epsilon_{xx}{}^{(n)} - n_{\text{eff}}{}^2 & \epsilon_{xy}{}^{(n)} & \epsilon_{xz}{}^{(n)} + n_{\text{eff}}N_x{}^{(n)} \\ \epsilon_{yx}{}^{(n)} & \epsilon_{yy}{}^{(n)} - n_{\text{eff}}{}^2 - N_x{}^{(n)2} & \epsilon_{yz}{}^{(n)} \\ \epsilon_{zx}{}^{(n)} + n_{\text{eff}}N_x{}^{(n)} & \epsilon_{zy}{}^{(n)} & \epsilon_{zz}{}^{(n)} - N_x{}^{(n)2} \end{bmatrix}\begin{bmatrix} E_{0x}{}^{(n)} \\ E_{0y}{}^{(n)} \\ E_{0z}{}^{(n)} \end{bmatrix} = 0. \tag{4}$$

For nontrivial plane-wave solutions, the determinant of the matrix in Eqs. (2) and (4) has to be zero[23,28]:

$$\det\{\hat{\mathbf{N}}^{(n)}[\hat{\mu}^{(n)}]^{-1}\hat{\mathbf{N}}^{(n)} + \hat{\epsilon}^{(n)}\} = 0, \tag{5}$$

which results in a fourth-order equation in $N_x{}^{(n)}$, which yields four roots: $N_{xj}{}^{(n)}$, $j = 1, 2, 3, 4$. This solution corresponds to four propagated waves called the eigenmodes. The eigenmodes that correspond to $N_{x1,3}{}^{(n)}$ are chosen as forward propagating waves; those that correspond to $N_{x2,4}{}^{(n)}$, as backward propagating waves (see Fig. 4). The terms "forward" and "backward" here are to be interpreted with respect to the x axis and obviously do not refer to the propagation direction of the sought waveguide eigenmodes. Solution of Eq. (4) gives for each $N_{xj}{}^{(n)}$ the corresponding electric-field vector amplitude, which can be written in the form $\mathbf{E}_{0j}{}^{(n)} = A_j{}^{(n)}\mathbf{e}_j{}^{(n)}$, where $A_j{}^{(n)}$ denotes the complex amplitude and $\mathbf{e}_j{}^{(n)}$ is the normalized eigenmode polarization. Similarly, by using Eqs. (1), one can obtain eigenmode magnetic-field vectors $\mathbf{H}_{0j}{}^{(n)}$ and $\mathbf{h}_j{}^{(n)}$.

The requirement for the continuity of the tangential components of the total electric field and the total magnetic field at the interfaces can be written in the form of 4×4 matrix equations.[25,23,28] The field amplitudes at the interfaces between the layered structure and the isotropic half-spaces at $x = x_0$ and $x = x_N$ are related by

$$\mathbf{A}^{(0)} = [\mathbf{D}^{(0)}]^{-1}\mathbf{D}^{(1)}\mathbf{P}^{(1)}[\mathbf{D}^{(1)}]^{-1} \ldots [\mathbf{D}^{(\mathcal{N})}]^{-1}\mathbf{D}^{(\mathcal{N}+1)}\mathbf{A}^{(\mathcal{N}+1)} = \mathbf{M}\mathbf{A}^{(\mathcal{N}+1)}, \tag{6}$$

where $\mathbf{A}^{(n)}$ is a four-component vector of the complex amplitudes $A_j{}^{(n)}$ of the jth ($j = 1, 2, 3, 4$) eigenmode in layer n:

$$\mathbf{A}^{(n)} = \begin{bmatrix} A_1{}^{(n)} \\ A_2{}^{(n)} \\ A_3{}^{(n)} \\ A_4{}^{(n)} \end{bmatrix}, \tag{7}$$

$\mathbf{D}^{(n)}$ is the 4×4 dynamic matrix:

$$\mathbf{D}^{(n)} = \begin{bmatrix} \mathbf{e}_{1y}{}^{(n)} & \mathbf{e}_{2y}{}^{(n)} & \mathbf{e}_{3y}{}^{(n)} & \mathbf{e}_{4y}{}^{(n)} \\ \mathbf{h}_{1z}{}^{(n)} & \mathbf{h}_{2z}{}^{(n)} & \mathbf{h}_{3z}{}^{(n)} & \mathbf{h}_{4z}{}^{(n)} \\ \mathbf{e}_{1z}{}^{(n)} & \mathbf{e}_{2z}{}^{(n)} & \mathbf{e}_{3z}{}^{(n)} & \mathbf{e}_{4z}{}^{(n)} \\ \mathbf{h}_{1y}{}^{(n)} & \mathbf{h}_{2y}{}^{(n)} & \mathbf{h}_{3y}{}^{(n)} & \mathbf{h}_{4y}{}^{(n)} \end{bmatrix}, \tag{8}$$

and $\mathbf{P}^{(n)}$ is the diagonal propagation matrix with diagonal elements $P_{ii}{}^{(n)} = \exp[-jk_0N_{xi}{}^{(n)}t_n]$, $i = 1, \ldots, 4$. The $\mathbf{M}$ matrix defined by Eq. (6) describes the global reflection and transmission properties of the layer structure.[25,23,29] It is useful to define the characteristic matrix[30,31]

$$\mathbf{S}^{(n)} = \mathbf{D}^{(n)}\mathbf{P}^{(n)}[\mathbf{D}^{(n)}]^{-1} \tag{9}$$

and express the $\mathbf{M}$ matrix of the structure as

$$\mathbf{M} = [\mathbf{D}^{(0)}]^{-1}\left[\prod_{n=1}^{\mathcal{N}}\mathbf{S}^{(n)}\right]\mathbf{D}^{(\mathcal{N}+1)}. \tag{10}$$

The optical intensity (power per unit area) of the jth plane-wave eigenmode in layer n is given by the amplitude of the Poynting vector:

$$S_j{}^n = \frac{1}{2}\Re[\mathbf{E}_{0j}{}^{(n)} \times \mathbf{H}_{0j}{}^{(n)*}]\exp\{2k_0\ \Im[N_{xj}{}^{(n)}]x\}. \tag{11}$$

The wave function of a guided mode must be a continuous, single-valued, and finite solution throughout the entire space. Consequently, only the amplitudes of the modes in the substrate and the superstrate for which the field decays to zero at $x = \mp\infty$ do not vanish (Fig. 2). If, for each layer, the eigenmodes are ordered in the following way:

$$\Im(N_{x1}) > 0, \qquad \Im(N_{x2}) < 0, \qquad \Im(N_{x3}) > 0,$$

$$\Im(N_{x4}) < 0, \tag{12}$$

complex amplitudes $A_1^{(0)} = A_3^{(0)} = A_2^{(\mathcal{N}+1)} = A_4^{(\mathcal{N}+1)} = 0$ will vanish according to Eq. (11) and Eq. (6) will become

$$\begin{bmatrix} 0 \\ A_2^{(0)} \\ 0 \\ A_4^{(0)} \end{bmatrix} = \begin{bmatrix} M_{11} & M_{12} & M_{13} & M_{14} \\ M_{21} & M_{22} & M_{23} & M_{24} \\ M_{31} & M_{32} & M_{33} & M_{34} \\ M_{41} & M_{42} & M_{43} & M_{44} \end{bmatrix} \begin{bmatrix} A_1^{(\mathcal{N}+1)} \\ 0 \\ A_3^{(\mathcal{N}+1)} \\ 0 \end{bmatrix}, \tag{13}$$

which finally results in the guided mode condition

$$M_{11}M_{33} - M_{13}M_{31} = 0. \tag{14}$$

Waveguide-mode condition (14) corresponds to the poles of reflectance amplitudes as originally derived by Yeh.[25] Note that the condition of the guided modes can be expressed in the form of Eq. (14) only if conditions (12) are satisfied.

2. *Magneto-Optical Transverse Geometry*

The calculation simplifies in the case of transverse MO geometry (magnetization vector parallel to the x axis). The relative permittivity tensor then has the following form[32]:

$$\hat{\epsilon}^{(n)} = \begin{bmatrix} \epsilon^{(n)} & 0 & -jQ^{(n)}\epsilon^{(n)} \\ 0 & \epsilon^{(n)} & 0 \\ jQ^{(n)}\epsilon^{(n)} & 0 & \epsilon^{(n)} \end{bmatrix}, \tag{15}$$

where $Q^{(n)}$ denotes the Voigt MO parameter, $\epsilon^{(n)} = n^{(n)2}$, and $n^{(n)}$ is the refractive index. The symmetry properties of tensor (15) are related to Onsager's principle, $\epsilon_{ij}(\mathbf{M}) = \epsilon_{ji}(-\mathbf{M})$, corresponding to the unique nonreciprocity of MO effects and resulting in device isolation. The off-diagonal components and MO parameter $Q^{(n)}$ are proportional to the transverse magnetization. Eigenvalue Eq. (5) simplifies to

$$[\epsilon^{(n)} - n_{\text{eff}}^2 - N_{x1,2}^{(n)2}] \times [\epsilon^{(n)} - Q^{(n)2}\epsilon^{(n)} - n_{\text{eff}}^2 - N_{x3,4}^{(n)2}] = 0. \tag{16}$$

There are four propagating eigenmodes in a transverse MO medium:

$$N_{x1}^{(n)} = -[\epsilon^{(n)} - n_{\text{eff}}^2]^{1/2}, \qquad \mathbf{e}_1^{(n)} = \begin{bmatrix} 0 \\ 1 \\ 0 \end{bmatrix}, \tag{17}$$

$$N_{x2}^{(n)} = -N_{x1}^{(n)}, \qquad \mathbf{e}_2^{(n)} = \begin{bmatrix} 0 \\ 1 \\ 0 \end{bmatrix}, \tag{18}$$

$$N_{x3}^{(n)} = -[\epsilon^{(n)} - n_{\text{eff}}^2 - Q^{(n)2}\epsilon^{(n)}]^{1/2},$$

$$\mathbf{e}_3^{(n)} = C_3^{(n)} \begin{bmatrix} jQ^{(n)}\epsilon^{(n)} - n_{\text{eff}}N_{x3}^{(n)} \\ 0 \\ \epsilon^{(n)} - n_{\text{eff}}^2 \end{bmatrix}, \tag{19}$$

$$N_{x4}^{(n)} = -N_{x3}^{(n)}, \qquad \mathbf{e}_4^{(n)} = C_4^{(n)} \times \begin{bmatrix} jQ^{(n)}\epsilon^{(n)} + n_{\text{eff}}N_{x3}^{(n)} \\ 0 \\ \epsilon^{(n)} - n_{\text{eff}}^2 \end{bmatrix}, \tag{20}$$

where $C_{3,4}^{(n)}$ are the normalization coefficients that correspond to the normalization condition. The dynamic matrix is in the block-diagonal form

$$\mathbf{D}^{(n)} = \begin{bmatrix} D_{11}^{(n)} & D_{11}^{(n)} & 0 & 0 \\ D_{21}^{(n)} & -D_{21}^{(n)} & 0 & 0 \\ 0 & 0 & D_{33}^{(n)} & D_{33}^{(n)} \\ 0 & 0 & D_{43}^{(n)} & D_{44}^{(n)} \end{bmatrix}, \tag{21}$$

where

$$D_{11}^{(n)} = 1,$$

$$D_{21}^{(n)} = N_{x1}^{(n)},$$

$$D_{33}^{(n)} = \epsilon^{(n)} - n_{\text{eff}}^2,$$

$$D_{43}^{(n)} = jQ^{(n)}\epsilon^{(n)}n_{\text{eff}} - \epsilon^{(n)}N_{x3}^{(n)},$$

$$D_{44}^{(n)} = jQ^{(n)}\epsilon^{(n)}n_{\text{eff}} + \epsilon^{(n)}N_{x3}^{(n)}.$$

The dynamic matrix for a nonmagnetic isotropic medium can be obtained from Eq. (21) by the substitution $Q = 0$. The two separate blocks in dynamic matrix (21) correspond to s polarization (TE) and p polarization (TM). TE and TM modes propagate independently, and no mode conversion occurs in the transverse MO geometry.[29,33] Consequently, total matrix $\mathbf{M}$ also becomes a block diagonal, and $M_{13} = M_{31} = 0$. In the linear approximation of the permittivity tensor, only p-polarized waves are sensitive to the transverse magnetization, and waveguide condition (14) for these modes takes the simple form $M_{33} = 0$.

3. *Numerical Implementation of Yeh's Algebra for a Waveguide Isolator*

Figure 4 shows schematically how waveguide condition term $M_{11}M_{33} - M_{13}M_{31}$ is obtained from a known complex propagation constant $n_{\text{eff}} = k_z/k_0$. However, modeling of the practical MO waveguide isolator requires calculation of the real and the imaginary parts of n_{eff} from a known waveguide geometry, which represents a numerical solution of the inverse problem. The waveguide resonant equation is solved by two-dimensional zero searching in the complex plane $[\Re(n_{\text{eff}}), \Im(n_{\text{eff}})]$. The problem is solved numerically as a two-dimensional minimization of the waveguide term amplitude by use of a Levenberg–Marquardt algorithm[34] with $\Re(n_{\text{eff}})$ and $\Im(n_{\text{eff}})$ as two fitting parameters. $\Re(n_{\text{eff}})$ is the propagation constant of the waveguide mode. According to the sign convention used, positive and negative $\Im(n_{\text{eff}})$ indicate an amplifying and a decaying waveguide mode, respectively.

The modal gain and the modal loss of the waveguide isolator are usually expressed in units of 1/cm or in decibels per centimeter. The gain in units of 1/cm can be obtained from the relation

$$\text{gain } [1/\text{cm}] = 2\frac{2\pi}{\lambda\ [\text{m}]}\frac{\Im(n_{\text{eff}})}{100} = 0.12566\frac{\Im(n_{\text{eff}})}{\lambda\ [\text{m}]}. \tag{22}$$

The factor 2 in Eq. (22) originates from power gain. Similarly, the gain in decibels per centimeter can be obtained from the relation

$$\text{gain } [\text{dB/cm}] = \frac{10}{\ln 10}\text{gain } [1/\text{cm}] = 0.5458\frac{\Im(n_{\text{eff}})}{\lambda\ [\text{m}]}. \tag{23}$$

B. First-Order Perturbation Theory

If it is assumed that the off-diagonal elements in relative permittivity tensor $\hat{\epsilon}$ of the MO ferromagnetic metal layer are small compared with the diagonal relative permittivities, then the TM eigenspectrum, i.e., eigenvalues and eigenfunctions (modal profiles), of the transversely magnetized MO waveguide can be deduced from the eigenspectrum of the isotropic waveguide by means of perturbation techniques. In this subsection we derive the perturbation formulas for this purpose. It must be noted that derivation of these formulas must be done with great care, as the unperturbed eigenspectrum is not power orthogonal, because of the metal losses that are already present in the unperturbed waveguide. As a result the perturbation formulas do not bear any resemblance to those traditionally encountered when one is calculating, for instance, modal gain in laser structures[35] or nonreciprocal TM phase shifts in yttrium iron garnet–based MO waveguides.[36] In those cases the original modal spectrum can be orthogonalized by use of the power integral of the modes, as the unperturbed waveguide is lossless. The derivation given here is more general and is correct for both lossy and lossless unperturbed waveguides, as it makes use of the fundamental Lorentz reciprocity theorem for the orthogonalization of the original modal spectrum.

1. *Modal Expansion for the Perturbed Fields*

The derivation of the perturbation formulas is based on the so-called modal expansion method.[37] The basic idea behind this approach is the completeness of the eigenspectrum of any isotropic waveguide.[38] As a result, the unknown eigenmode $\{\mathbf{E}(\mathbf{r}), \mathbf{H}(\mathbf{r})\}$ of the actual MO waveguide can be expanded in the complete set $\{\mathbf{E}_i(\mathbf{r}), \mathbf{H}_i(\mathbf{r})\}$ formed by the eigenmodes of the unperturbed, isotropic waveguide. Throughout this section, capital letters are used to represent the modal fields including their z-dependent propagation factors $\exp(-j\beta_i z)$, whereas lowercase letters are used to describe the field profiles (and thus depend only on transversal coordinates $\boldsymbol{\rho}$).

The Maxwell equations in the perturbed waveguide can be put in the form

$$\begin{aligned}\nabla \times \mathbf{E}(\mathbf{r}) &= -j\omega\mu_0\mathbf{H}(\mathbf{r}),\\ \nabla \times \mathbf{H}(\mathbf{r}) &= j\omega\epsilon_0\epsilon_r(\boldsymbol{\rho})\mathbf{E}(\mathbf{r}) + \mathbf{J}(\mathbf{r}),\end{aligned} \tag{24}$$

where

$$\mathbf{J}(\mathbf{r}) = j\omega\epsilon_0\Delta\hat{\epsilon}(\boldsymbol{\rho}) \cdot \mathbf{E}(\mathbf{r}), \tag{25}$$

$$\Delta\hat{\epsilon}(\boldsymbol{\rho}) = \begin{bmatrix} 0 & 0 & -j\epsilon_r Q \\ 0 & 0 & 0 \\ +j\epsilon_r Q & 0 & 0 \end{bmatrix}. \tag{26}$$

In other words, the perturbation can be written as a current source term for the unperturbed waveguide. Using the completeness theorem, we can expand the transversal components of the unknown fields as (where $\mathcal{M}$ is the full eigenmode set of the unperturbed waveguide, including both forward and backward propagating modes):

$$\begin{bmatrix}\mathbf{E}_t(\mathbf{r})\\ \mathbf{H}_t(\mathbf{r})\end{bmatrix} = \sum_{i\in\mathcal{M}} C_i(z)\begin{bmatrix}\mathbf{E}_{t,i}(\mathbf{r})\\ \mathbf{H}_{t,i}(\mathbf{r})\end{bmatrix}, \tag{27}$$

where a z dependence of the C expansion coefficients is allowed.

A similar expansion equation can now be derived for the longitudinal components of the unknown fields by use of the z components of the Maxwell curl equations:

$$\begin{aligned}\mathbf{u}_z \cdot [\nabla_t \times \mathbf{E}_t(\mathbf{r})] &= -\nabla_t \cdot [\mathbf{u}_z \times \mathbf{E}_t(\mathbf{r})]\\ &= -j\omega\mu_0 H_z(\mathbf{r}),\\ \mathbf{u}_z \cdot [\nabla_t \times \mathbf{H}_t(\mathbf{r})] &= -\nabla_t \cdot [\mathbf{u}_z \times \mathbf{H}_t(\mathbf{r})]\\ &= j\omega\epsilon_0\mathbf{u}_z \cdot [\epsilon_r(\boldsymbol{\rho})\hat{I} + \Delta\hat{\epsilon}(\boldsymbol{\rho})]\\ &\quad \cdot \mathbf{E}(\mathbf{r}),\end{aligned} \tag{28}$$

where $\hat{I}$ is the 3×3 unity tensor.

The same equations but without the perturbation are satisfied by the modal fields of the isotropic waveguide:

$$\begin{aligned}-\nabla_t \cdot [\mathbf{u}_z \times \mathbf{E}_{t,i}(\mathbf{r})] &= -j\omega\mu_0 H_{z,i}(\mathbf{r}),\\ -\nabla_t \cdot [\mathbf{u}_z \times \mathbf{H}_{t,i}(\mathbf{r})] &= j\omega\epsilon_0\epsilon_r(\boldsymbol{\rho})E_{z,i}(\mathbf{r}).\end{aligned} \tag{29}$$

If the transversal expansions of Eq. (27) are substituted into Eqs. (28), making use of Eqs. (29) and expanding the right-hand part of the second of Eqs. (28) in its longitudinal and transversal contributions yield the following expansion formulas for the longitudinal parts of the unknown fields:

$$\begin{aligned}H_z(\mathbf{r}) &= \sum_{i\in\mathcal{M}} C_i(z)H_{z,i}(\mathbf{r}),\\ E_z(\mathbf{r}) &= \frac{1}{j\omega\epsilon_0\epsilon_r(\boldsymbol{\rho})}\Bigg\{-\sum_{i\in\mathcal{M}} C_i(z)\nabla_t \cdot [\mathbf{u}_z \times \mathbf{H}_{t,i}(\mathbf{r})]\\ &\quad - j\omega\epsilon_0\sum_{i\in\mathcal{M}} C_i(z)\Delta\hat{\epsilon}_{zt}(\boldsymbol{\rho}) \cdot \mathbf{E}_{t,i}(\mathbf{r})\Bigg\}\\ &= \sum_{i\in\mathcal{M}} C_i(z)E_{z,i} - \sum_{i\in\mathcal{M}} C_i(z)\frac{\Delta\hat{\epsilon}_{zt}(\boldsymbol{\rho})}{\epsilon_r(\boldsymbol{\rho})} \cdot \mathbf{E}_{t,i}(\mathbf{r}).\end{aligned} \tag{30}$$

Here it is assumed that summation and differentiation can be interchanged. Now the problem is reduced to finding a set of scalar expansion coefficients $C_i(z)$ instead of three-dimensional unknown fields $\{\mathbf{E}(\mathbf{r}), \mathbf{H}(\mathbf{r})\}$.

The next step in the derivation of the perturbation formulas consists of building a set of coupled first-order differential equations for $C_i(z)$. For this purpose we first need to take a small sidestep and recall the orthogonality relationships that are satisfied by the modes of the lossy unperturbed waveguide. It is known that for a lossy iso-

tropic waveguide the orthogonality between the eigenmodes is expressed through the field integral

$$\frac{1}{2}\int\int [\mathbf{e}_i(\boldsymbol{\rho}) \times \mathbf{h}_j(\boldsymbol{\rho})] \cdot \mathbf{u}_z \mathrm{d}S = \delta_{ij}, \tag{31}$$

or, by use of the mirroring properties ($\mathbf{e}_{t,i} = \mathbf{e}_{t,-i}$ and $\mathbf{h}_{t,i} = -\mathbf{h}_{t,-i}$) of isotropic waveguides and noting that only transversal field components contribute to the integral in Eq. (31),

$$\frac{1}{4}\int\int [\mathbf{e}_{-i}(\boldsymbol{\rho}) \times \mathbf{h}_j(\boldsymbol{\rho}) - \mathbf{e}_j(\boldsymbol{\rho}) \times \mathbf{h}_{-i}(\boldsymbol{\rho})] \cdot \mathbf{u}_z \mathrm{d}S = \delta_{ij}. \tag{32}$$

Note that, in this version, the z-independent modal field profiles $\{\mathbf{e}_i(\boldsymbol{\rho}), \mathbf{h}_i(\boldsymbol{\rho})\}$ can be replaced by their z-dependent counterparts $\{\mathbf{E}_i(\mathbf{r}), \mathbf{H}_i(\mathbf{r})\}$, because each term represents a multiplication of a forward- and backward-traveling mode, so the exponential propagator factors will cancel. One can determine the expansion coefficients $C_i(z)$ by projecting $\{\mathbf{E}(\mathbf{r}), \mathbf{H}(\mathbf{r})\}$ onto the eigenmodes of the unperturbed waveguide $\{\mathbf{E}_j(\mathbf{r}), \mathbf{H}_j(\mathbf{r})\}$ and using Eq. (32):

$$C_i(z) = \frac{1}{4}\int\int [\mathbf{E}_{-i}(\mathbf{r}) \times \mathbf{H}(\mathbf{r}) - \mathbf{E}(\mathbf{r}) \times \mathbf{H}_{-i}(\mathbf{r})] \cdot \mathbf{u}_z \mathrm{d}S. \tag{33}$$

Now we are close to the announced set of coupled differential equations for $C_i(z)$. The last step consists of deriving the connection between perturbation current source $\mathbf{J}$ of Eq. (25) and the expansion coefficients $C_i(z)$. Such a relationship will express the way in which the perturbation current source excites the different unperturbed modes.

This connection can be found by use of the fundamental Lorentz reciprocity theorem.[38] The normal eigenmode $\{\mathbf{E}_j(\mathbf{r}), \mathbf{H}_j(\mathbf{r})\}$ is sustained in the unperturbed waveguide without any sources, whereas the unknown fields $\{\mathbf{E}(\mathbf{r}), \mathbf{H}(\mathbf{r})\}$ are, according to Eqs. (24), sustained in the unperturbed waveguide by the current source $\mathbf{J}(\mathbf{r})$ of Eq. (25). Applying the Lorentz reciprocity theorem to these two sets of fields yields

$$\nabla \cdot [\mathbf{E}_{-i}(\mathbf{r}) \times \mathbf{H}(\mathbf{r}) - \mathbf{E}(\mathbf{r}) \times \mathbf{H}_{-i}(\mathbf{r})] = -\mathbf{E}_{-i}(\mathbf{r}) \cdot \mathbf{J}(\mathbf{r}). \tag{34}$$

Integrating Eq. (34) over an arbitrary cross section of the waveguide gives

$$\int\int \left\{\nabla_t \cdot [\mathbf{E}_{-i}(\mathbf{r}) \times \mathbf{H}(\mathbf{r}) - \mathbf{E}(\mathbf{r}) \times \mathbf{H}_{-i}(\mathbf{r})] + \frac{\mathrm{d}}{\mathrm{d}z}[\mathbf{E}_{-i}(\mathbf{r}) \times \mathbf{H}(\mathbf{r}) - \mathbf{E}(\mathbf{r}) \times \mathbf{H}_{-i}(\mathbf{r})] \cdot \mathbf{u}_z\right\} \mathrm{d}S = \int\int \mathbf{E}_{-i}(\mathbf{r}) \cdot \mathbf{J}(\mathbf{r}) \mathrm{d}S. \tag{35}$$

The first term on the left-hand side of Eq. (35) reduces to a contour integral at infinity by means of a Green integral theorem, which will, owing to the radiation boundary condition, be zero, whereas the second term is (if integration and differentiation are interchangeable) in view of Eq. (33) nothing else but four times the z derivative of the $C_i(z)$ coefficient. Expanding perturbation current source $\mathbf{J}$ by use of Eqs. (27) and (30) and taking the form of the permittivity perturbation [Eq. (26)] into account yield

$$\mathbf{J} = j\omega\epsilon_0\epsilon_r(\boldsymbol{\rho})Q(\boldsymbol{\rho}) \sum_{k \in \mathcal{M}} C_k(z)[jE_{x,k}(\mathbf{r})\mathbf{u}_z - jE_{z,k}(\mathbf{r})\mathbf{u}_x - Q(\boldsymbol{\rho})E_{x,k}(\mathbf{r})\mathbf{u}_x]. \tag{36}$$

This equation yields the announced set of coupled first-order differential equations:

$$\frac{\mathrm{d}C_i(z)}{\mathrm{d}z} = -j\sum_{k \in \mathcal{M}} A_{ik}C_k(z)\exp[-j(\beta_k - \beta_i)z], \tag{37}$$

with ($\mathbf{e}_{t,i} = \mathbf{e}_{t,-i}$ and $e_{z,i} = -e_{z,-i}$)

$$A_{ik} = -j\frac{\omega\epsilon_0}{4}\int\int \{\epsilon_r(\boldsymbol{\rho})Q(\boldsymbol{\rho})[e_{z,i}(\boldsymbol{\rho})e_{x,k}(\boldsymbol{\rho}) + e_{x,i}(\boldsymbol{\rho})e_{z,k}(\boldsymbol{\rho}) - jQ(\boldsymbol{\rho})e_{x,i}(\boldsymbol{\rho})e_{x,k}(\boldsymbol{\rho})]\}\mathrm{d}S. \tag{38}$$

Incorporating the propagator factor in the z-dependent expansion coefficients, $X_i(z) = C_i(z)\exp(-j\beta_i z)$, results in the following compact version of the evolution equations:

$$\frac{\mathrm{d}X_i(z)}{\mathrm{d}z} = -j\beta_i X_i(z) - j\sum_{k \in \mathcal{M}} A_{ik}X_k(z). \tag{39}$$

It is important to note that, until now, no approximations have been made. The set of evolution equations above is a rigorously equivalent formulation of the Maxwell equations for the unknown electromagnetic fields.

2. *First-Order Perturbation Formulas*

The set of evolution equations described by Eq. (39) represents nothing else but the eigensystem for the modes of the MO waveguide. Indeed, Eq. (39) can, in matrix notation, be written as

$$\frac{\mathrm{d}\bar{\bar{X}}(z)}{\mathrm{d}z} = -j\bar{\bar{A}} \cdot \bar{\bar{X}}(z), \tag{40}$$

with

$$\bar{\bar{A}}_{ik} = \beta_i\bar{\bar{I}} + \bar{\bar{A}}_{ik}. \tag{41}$$

Solving for the eigenmodes of the MO waveguide thus gets down to calculating the eigenvalues Γ and the eigenvectors $\mathcal{A}$. The practical problem generally consists of evaluating the modification of the eigenvalue and the eigenfunction (modal profile) of an unperturbed guided mode m caused by the perturbation. Within the assumption of weak perturbation, this problem can be formally solved by means of an iteration procedure. In the limit of a vanishing perturbation, we must recover mode m, i.e., $\Gamma = \beta_m$, $X_m = 1$ [the $\exp(-j\Gamma z)$ dependence is henceforth understood], and $X_i = 0$ for $i \neq m$. For a nonzero perturbation we keep $X_m = 1$ and assume that $\Gamma - \beta_m$ and that the other X_i are of order $\mathcal{O}(1)$. Up to first order in the perturbation, Eq. (39) then reads as

$$\Gamma - \beta_m = A_{mm} + \mathcal{O}(2), \tag{42a}$$

$$(\Gamma - \beta_i)X_i = A_{im} + \mathcal{O}(2), \qquad i \neq m, \tag{42b}$$

or, up to first order,

$$X_i = \frac{A_{im}}{\beta_m - \beta_i}, \qquad i \neq m. \tag{42c}$$

For the particular MO waveguide under study here, the first-order perturbation shift of the propagation constant of guided mode m thus becomes

$$\Delta\beta_m = -j\frac{\omega\epsilon_0}{2}\int\int \epsilon_r(\boldsymbol{\rho})Q(\boldsymbol{\rho})e_{x,m}(\boldsymbol{\rho})e_{z,m}(\boldsymbol{\rho})\mathrm{d}S$$

$$= \frac{\omega\epsilon_0}{2}\int\int \Delta\hat{\epsilon}_{xz}(\boldsymbol{\rho})e_{x,m}(\boldsymbol{\rho})e_{z,m}(\boldsymbol{\rho})\mathrm{d}S. \tag{43}$$

Note that the last term in the integrand of Eq. (38) has been neglected for the calculation of A_{mm}, as it is of second order in Q. Here it is tacitly assumed that the unperturbed guided mode is normalized according to Eq. (31). Remarking that $e_{z,-m} = -e_{z,m}$ and $e_{x,-m} = e_{x,m}$ proves that this shift $\Delta\beta$ is indeed nonreciprocal. Furthermore, using the second form of Eq. (43) easily shows that in the case of a lossless waveguide the nonreciprocal phase shift is purely real. Indeed, for a lossless waveguide, $\Delta\hat{\epsilon}_{xz}$ is purely imaginary (because of the needed hermiticity of the permittivity tensor) and, as is known from optical waveguide theory, e_x and e_z are exactly $\pi/2$ out of phase. The integrand in the second form of Eq. (43) is thus purely real, because, except for a trivial normalization constant, e_x can be chosen to be purely real. When the waveguide becomes lossy, $\Delta\beta$ acquires an important imaginary part, owing both to a small change in the $\pi/2$ phase difference between e_x and e_z and, more importantly, to the occurrence of a nonzero real part for $\Delta\epsilon_{xz}$ (breaking the hermiticity of the permittivity tensor of the MO layer).

The first-order correction to the modal profile of the guided modes can be only approximatively calculated with Eq. (42c), as it requires not only a discretization of the continuum of radiation modes but also a truncation of that discretized part of the spectrum. In that way the practical value of Eq. (42c) is quite limited. The main feature of perturbation theory modeling of this device lies in its straightforward calculation of the shift of the propagation constant. Finally, it has to be remarked that TE modes in this configuration can also experience a nonreciprocal phase shift. Indeed, a TE mode in an actual two-dimensional waveguide cross section does not have vanishing x and z components, and Eq. (43) will therefore not be strictly zero for TE modes (as it would for a slab waveguide). This phenomenon is, however, several orders of magnitude smaller than the standard TM nonreciprocal phase shift.

Using Eqs. (43) and (23), we can calculate the isolation ratio of the device, defined as the ratio of the extinction of forward optical power to backward optical power and expressed in decibels per centimeter as IS [dB/cm] $\simeq 17.37 \times \Im(\Delta\beta\,[1/\mathrm{cm}])$. The integral in Eq. (43) can easily be numerically evaluated by use of an extended Simpson quadrature formula, as for most practical situations the MO metal can be approximated by a rectangular region. For the calculation of the unperturbed field profiles there exists a variety of mode solvers that are capable of solving for fully vectorial field profiles of waveguides with one- or two-dimensional cross sections.

C. Advantages and Disadvantages of the Two Methods

The two theoretical models outlined above have fundamentally different approaches to the modeling of the device under study, which naturally implies that each has both advantages and disadvantages.

The method based on Yeh's matrix formalism is rigorous without approximations. For a transversal MO structure, the algebra becomes simple and the modeling difficulty is comparable with that of nonmagnetic structures. Other advantages of the Yeh formalism are (i) its easy generalization to MO waveguides with a general magnetization direction in specific polarization conversion waveguides, (ii) the possibility that it can include nonlinear terms that originate from higher-order MO tensors, (iii) the fact that a matrix-based method facilitates fast treatment of a periodic system, and (iv) its ability to be generalized to more-complex structures including optical anisotropy.

The main advantage of the perturbation method lies in the numerical effort required. The model requires a full vectorial TM modal solution of a one-dimensional isotropic waveguide (which is, with modern-day waveguide-solving tools, a straightforward task) combined with the numerical integration of a one-dimensional overlap integral. Unlike the perturbation method, the rigorous matrix formalism has to be exercised twice, once for the forward and once for the backward propagation direction. The main advantage of the perturbation model therefore is its modeling speed, interesting for a fast optimization of the device. However, calculation of the precise modal profiles of the MO waveguide is nearly impossible with the perturbation method, because of the infinite summation in Eq. (42c). Finally, an important advantage of the perturbation approach is that it is not restricted by the dimensionality or the shape of the perturbation region. As soon as the unperturbed nonmagnetic waveguide can be solved, the nonreciprocal phase shift can be calculated by evaluation of the overlap integral [Eq. (43)].

4. NUMERICAL MODELING

The two modeling approaches are numerically compared in a hypothetical benchmark example with a simplified layer structure. Even though the numerical results obtained for the internal gain levels needed in this structure are quantitatively close to or above the limit of what is possible, this example provides a qualitative insight into the behavior of the device. Furthermore, it allows us to draw important conclusions concerning the modeling approaches of this type of device. In Subsection 4.B the rigorous Yeh method is applied to a realistic MQW SOA layer structure to indicate the numerical feasibility of the concept and give some idea of the optimization routines used in the design of this type of nonreciprocal waveguide.

For all simulations the telecom wavelength of 1.3 μm was used, and an InP-based material system was chosen for the SOA layer structure. The isolator structure consists of a $Co_{90}Fe_{10}$ MO film with in-plane magnetic anisotropy at transversal geometry. We pragmatically introduce optical gain in the InGaAsP active layer(s) into the numerical model as a positive imaginary part for the medium's refractive index without modeling the relationship between carrier concentration and optical gain.

A. Simplified Isolator Structure

Figure 5 shows the simplified structure of the isolator consisting of a $Co_{90}Fe_{10}$ MO film, an InP spacer layer, and an InGaAsP layer that comprises an effective active medium upon an InP substrate. Optical constants of the materials and thicknesses are shown.[39–42]

Guided TM modes correspond to the zero points of the waveguide term [Eq. (14)], which for the transversal MO configuration reduces to $M_{33} = 0$. Figure 6 shows the dependence of waveguide term $|M_{33}|$ on the real and the imaginary parts of the effective index of refraction, $\Re(n_{\text{eff}})$ and $\Im(n_{\text{eff}})$. A sharp minimum (zero point) corresponds to zero-order guided mode TM_0. Searching for a minimum in the complex plane $[\Re(n_{\text{eff}}), \Im(n_{\text{eff}})]$ gives the solution of the waveguide resonant condition. Note that the waveguide term falls to zero also for n_{eff} equal to the substrate's refractive index. Consequently, minimum searching close to the cutoff condition (n_{eff} close to the substrate's refractive index) requires taking care of the numerical stability of the solution and a proper choice of the initial guess used in the minimization.

Figure 7 shows the modal gain $[\propto \Im(n_{\text{eff}})]$ of the zero-order TM mode as a function of the internal gain of the active layer. The difference between forward and backward regimes represents the nonreciprocal gain property of the transversal MO isolator. The gain and losses of the waveguide can be controlled by the internal gain of the active layer. If the waveguide gain is adjusted to zero for the forward direction, the loss in the backward direction will represent the desired device isolation. An almost linear dependence of the waveguide gain–losses in both directions enables a fast calculation to be made of the device's isolation and the necessary internal gain of the active layer.

Figures 8 and 9 show the dependence of the waveguide isolation and the necessary internal gain of the active layer on the thickness of the active layer. Isolation increases for decreasing active-layer thickness and reaches a maximum just above cutoff thickness. The steep decrease of isolation when the cutoff core thickness is approached is a result of a strong increase of the modal tail into the substrate when the mode approaches cutoff. As a consequence, the relative amount of guided TM light near the MO metal drops steeply. The increase in necessary internal gain of the active layer with decreasing active-layer thicknesses does not show this maximum. This is so because decreasing the active layer's thickness will only result in a smaller overlap with the gain region and hence will always lead to an increasing necessary internal gain. The dependencies for different thicknesses of the InP spacer layer show that both the isolation and the necessary internal gain of the active layer increase for

air	$n^{(0)} = 1$	
$Co_{90}Fe_{10}$ MO layer	$n^{(1)} = 4.35 - j4.75$ $Q = 0.0214 + j0.0442$	$t^{(1)} = 100$ nm
InP spacer layer	$n^{(2)} = 3.2019$	$t^{(2)} = 250$ nm
InGaAsP active layer	$n^{(3)} = 3.3971 + jk$	$t^{(3)} = 200$ nm
InP substrate	$n^{(4)} = 3.2019$	

Fig. 5. Multilayer structure of the waveguide isolator and the coordinate system chosen. Optical and MO constants for the wavelength of 1300 nm were obtained from Refs. 39–42.

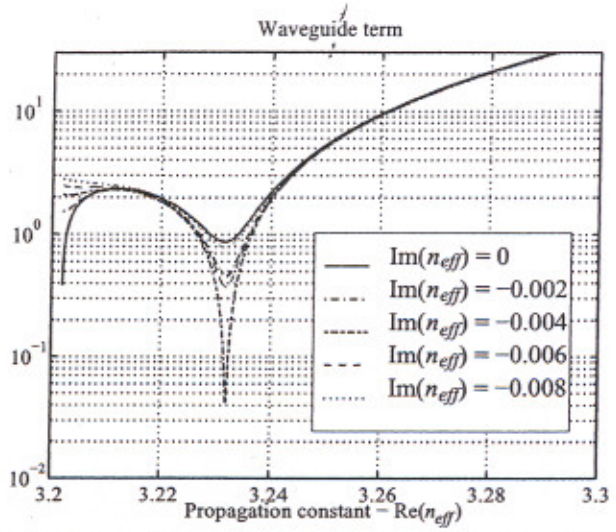

Fig. 6. Waveguide term $|M_{33}|$ as a function of $\Re(n_{\text{eff}})$ and $\Im(n_{\text{eff}})$ for the structure shown in Fig. 5. A thickness of the InP spacer layer of $t^{(2)} = 500$ nm and zero gain of the active layer $k = 0$ were used in the model. The sharp minimum corresponds to the guided mode that satisfies waveguide resonant condition $M_{33} = 0$. Searching the minimum of $|M_{33}|$ by use of the optimization algorithm gives the value $n_{\text{eff}} = 3.23195 - j0.00416$.

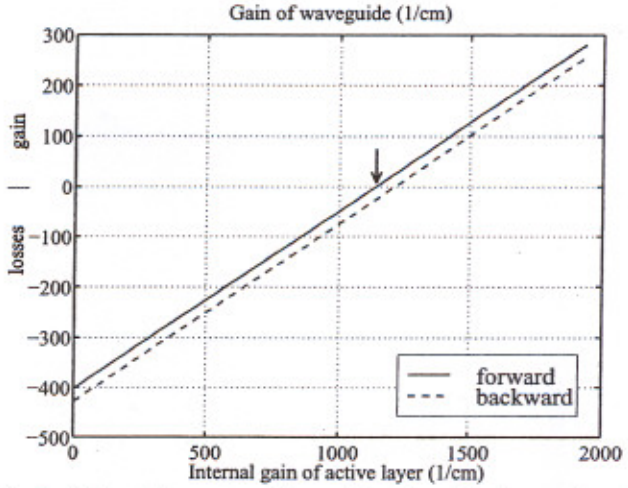

Fig. 7. Gain of the waveguide as a function of the internal gain of the active layer. The difference between forward and backward regimes represents nonreciprocal properties of the transversal MO isolator. The structure of the waveguide is the same as that shown in Fig. 5. Whereas the gain of the active layer was adjusted to 1139 cm^{-1} ($k = 0.01178$), the waveguide gain for the forward direction was equal to zero. Then the isolation of the device defined as backward losses was 24.4 cm^{-1} [corresponding to $\Im(n_{\text{eff}}) = 0.000252$].

decreasing InP spacer thickness. This is not a surprising result, as energy easily penetrates the thinner InP spacer into the absorbing MO layer. Consequently, if the maximum achievable internal gain for a fixed active layer thickness is known, one can optimize the isolation ratio of the device by optimizing the spacer layer's thickness within the limits of the available gain.

Figure 10 shows the effect of the MO layer's thickness. Both the isolation and the necessary gain of the active layer increase with increasing $Co_{90}Fe_{10}$ thickness. For large thicknesses the effect is saturated, indicating that the upper interface of the MO metal has become irrelevant. The existence of a maximum and the behavior for thin MO films originate from the effects of phase changes of reflected waves at the interfaces and interference phenomena.

All the simulations described above were performed with both Yeh's formalism and the perturbation theory model. The two approaches gave nearly identical outputs, indicating that the assumptions of perturbation theory are valid and the induced MO anisotropy can indeed be considered a weak perturbation. Another confirmation of this conclusion is given by Fig. 11. Here, waveguide isolation is plotted as a function of the strength of the Voigt MO parameter for various thicknesses of InP spacer layers. Very good agreement between models is obtained for the measured,[42] practical value of the parameter (factor $f = 1$). The small differences for a stronger MO parameter, i.e, higher off-diagonal elements of the permittivity tensor, originate from neglecting the nonlinear terms in Q in the perturbation-theory approach. The nonlinearity of the dependencies shown that were obtained with Yeh's formalism correspond to higher-order MO effects originating from linear MO tensor.[43] These small and negligible differences between the numerical results of the two models prove that for this device the perturbation-theory approach is suitable for fast optimization.

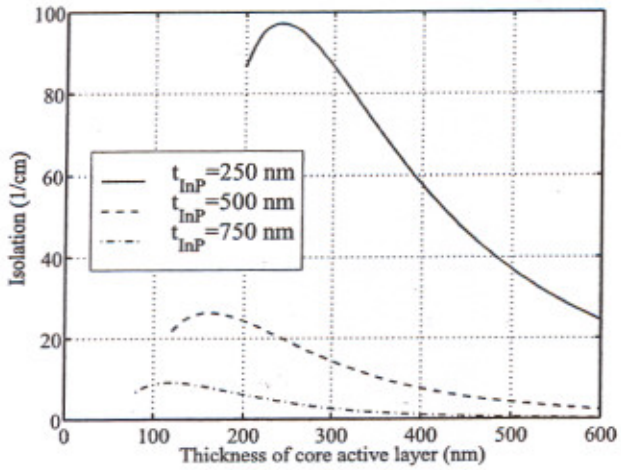

Fig. 8. Device isolation as a function of active-layer thickness shown for the waveguide structure from Fig. 5. The three curves correspond to InP spacer layer thicknesses of 250, 500, and 750 nm.

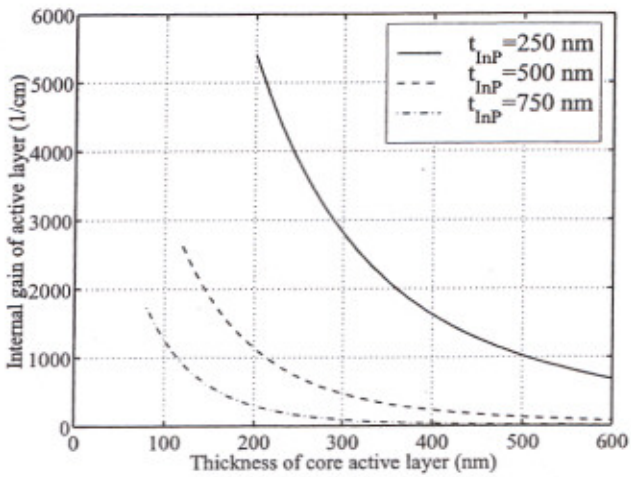

Fig. 9. Necessary internal gains of the active layer for compensation of waveguide absorption losses in the forward direction are shown for the same conditions as in Fig. 8.

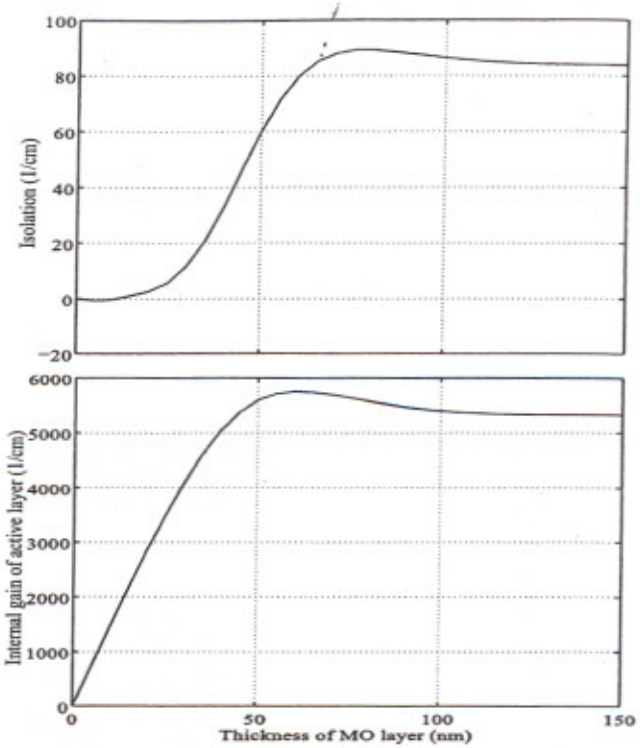

Fig. 10. Waveguide isolation and the necessary internal gains of the active layer as functions of MO layer thickness. The structure of the waveguide is the same as shown in Fig. 5.

The values for the necessary internal gain, obtained for this simplified isolator layer structure, are for some cases greater than what is theoretically achievable in bulk active layers. Therefore, the main goal of this example was to illustrate qualitatively the influence of the different structural parameters on the behavior of the device and to compare the two different modeling approaches. In Subsection 4.B it will be numerically shown that this device is indeed feasible if a tensile strained MQW layer structure is used.

B. Multiple-Quantum-Well-Based Isolator

The simplified MO waveguide of Subsection 4.A is generalized here to a more realistic MQW structure. Its details are summarized in Table 1, with the optical and MO parameters indicated. The active layer consists of a

multilayer of six tensile strained QWs separated by strain-compensating compressive strained barrier layers. The upper and lower separate confinement heterostructure (SCH) layers have been included to permit optimization of the TM confinement in the active region. The conducting semiconductor contact layers on top are needed to facilitate the formation of a good ohmic contact for the current injection.

Structure and layer thicknesses have to be optimized to maximize desired waveguide isolation for minimal, or at least achievable, internal gain of the QWs. Optimization of the structure can be obtained by nonlinear least-squares fitting of the thickness parameters. We propose the following merit function, which has to be minimized:

$$\text{Merit function} = \frac{\text{Internal gain}^{j}}{\text{Isolation}^{m}}, \tag{44}$$

where m is a constant that characterizes how much the influence of the gain in this merit function is limited.

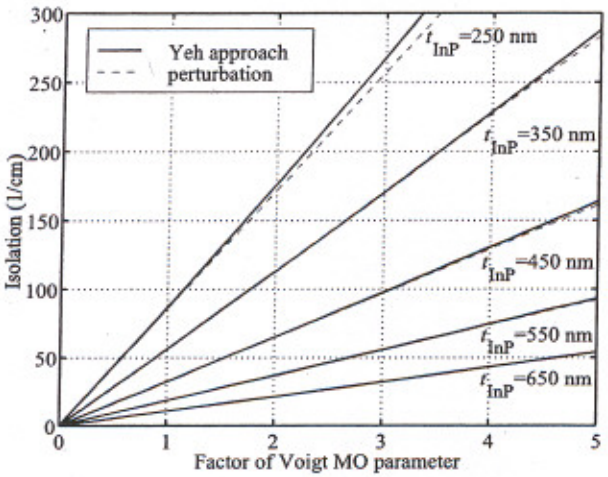

Fig. 11. Comparison of the perturbation theory and the rigorous approach based on Yeh's formalism. Waveguide isolation is shown as a function of the factor of Voigt MO parameter $Q' = fQ_{CoFe}$. The MO waveguide of a real $Co_{90}Fe_{10}$ film corresponds to $f = 1$. Good agreement between the two approaches can be observed.

Figure 12 shows the thicknesses optimization of the isolator structure shown in Table 1. First, the SCH layers were optimized by use of the merit function from Eq. (44) for the InP spacer thickness as a constant parameter. The factor $m = 1$ was chosen. In the second step we could choose the thickness of the InP spacer layer to use optimally the available gain of active layer. It can be seen how for increasing thickness of the InP spacer layer, or in other words for a layer structure converging toward a nonmagnetic waveguide, both SCH layers converge as expected toward the same value, resulting in a symmetrical guiding layer. For extremely thin InP spacer layers the role of the lower SCH layer becomes increasingly irrelevant. Figures 12(a) and 12(b) show that, for normal internal gain levels in the QWs, isolation ratios up to 30 cm^{-1} are achievable by this device. This means that, for instance, 25 dB of net isolation requires a device length of only 1.9 mm.

These preliminary practical device simulations prove the feasibility of the novel isolator concept. A more-detailed device optimization requires a thorough study of several other effects, such as the gain-current behavior of the active layer, the optimization of the number of wells with the distribution of the electrical carriers over the QWs taken into account, and optimization of the two-dimensional layout of the waveguide cross section with lateral current spreading taken into account. However, even though all these effects would permit a better optimization of the practical device layout, they will not change the order of magnitude of the isolation values predicted here or of the needed QW internal gain levels.

Table 1. Structure of the Modeled Isolator Based on Tensile Strained MQW Structure[a]

Layer	Composition (Dopant, Strain ϵ)	Refractive Index (Bandgap λ_g)	Thickness
MO layer	$Co_{90}Fe_{10}$	$n = 4.35 - j4.75$ ($Q = 0.0214 + j0.0442$)	100 nm
Absorbing contact layer	$In_{0.54}Ga_{0.46}As$ (Be: 3×10^{19} cm^{-3})	$n = 3.6 - j0.2$ (1.62 μm)	15 nm
Transparent contact layer	$In_{0.81}Ga_{0.19}As_{0.41}P_{0.59}$ (Be: 1×10^{19} cm^{-3})	$n = 3.37$ (1.17 μm)	100 nm
Spacer layer	InP	$n = 3.203$ (0.9 μm)	140–420 nm
Upper SCH	$In_{0.9}Ga_{0.1}As_{0.21}P_{0.79}$	$n = 3.28$ (1.03 μm)	Optimize
Barrier (×7)	$In_{0.93}Ga_{0.07}As_{0.22}P_{0.78}$ ($\epsilon = +0.2\%$)	$n = 3.29$ (1.06 μm)	22 nm
QW (×6)	$In_{0.48}Ga_{0.52}As_{0.78}P_{0.22}$ ($\epsilon = -1.1\%$)	$n = 3.34 + jk$ (1.3 μm)	11 nm
Lower SCH	$In_{0.9}Ga_{0.1}As_{0.21}P_{0.79}$	$n = 3.28$ (1.03 μm)	Optimize
Substrate	InP	$n = 3.203$ (0.9 μm)	

[a] Refractive indices are taken from Refs. 39–42.

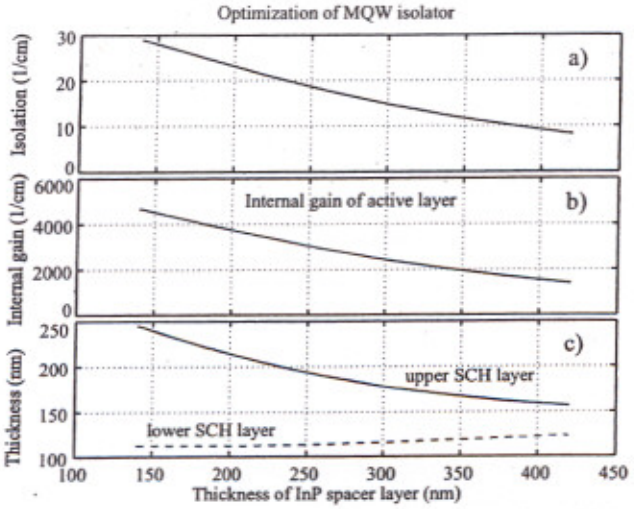

Fig. 12. Optimization of the MWQ-based isolator described in Table 1. The lower and upper SCH layers are optimized by use of the merit function from Eq. (44) with $m = 1$ for the InP spacer thickness as a constant parameter. For a given available internal gain of the QW structure (b), the optimal thicknesses of InP and SCH layers (c) can be obtained. (a), The corresponding isolation.

5. CONCLUSIONS

Application of the 4×4 Yeh matrix formalism to model the isolation properties of a novel magneto-optical integrated optical isolator has been demonstrated. The rigorous approach has been compared with the fast perturbation-theory method. Good agreement between the two approaches was obtained, proving the usefulness of approximate perturbation methods for these MO devices. Rigorous simulations and preliminary optimization of the one-dimensional layer structure of a practical tensile strained MQW CoFe-clad SOA prove the theoretical feasibility of this novel isolator concept.

ACKNOWLEDGMENTS

This study was done within the framework of Information Science Technologies project IST-Isolaser of the European Commission (IST-2001-37854). Partial support from the Grant Agency of the Czech Republic (202/03/0776) and the Nanomag-lab project of the European Commission (Marie Curie Host Fellowships for Transfer of Knowledge, 2004-003177) is acknowledged.

REFERENCES

1. M. Levy, "The on-chip integration of magnetooptic waveguide isolators," IEEE J. Sel. Top. Quantum Electron. **8**, 1300–1306 (2002).
2. M. Levy, R. Scarmozzino, R. M. Osgood, Jr., R. Wolfe, F. J. Cadieu, H. Hedge, C. J. Gutierrez, and G. A. Prinz, "Permanent magnet film magneto-optic waveguide isolator," J. Appl. Phys. **75**, 6286–6288 (1994).
3. H. Yokoi, T. Mizumoto, S. Kuroda, T. Ohtsuka, and Y. Nakano, "Elimination of a back-reflected TE mode in a TM-mode optical isolator with Mach–Zehnder interferometer," Appl. Opt. **41**, 7045–7051 (2002).
4. H. Yokoi, T. Mizumoto, and Y. Shoji, "Optical nonreciprocal devices with a silicon guiding layer fabricated by wafer bonding," Appl. Opt. **42**, 6605–6612 (2003).
5. J. Fujita, M. Levy, R. M. Osgood, Jr., L. Wilkens, and H. Dötsch, "Waveguide optical isolator based on Mach–Zehnder interferometer," Appl. Phys. Lett. **76**, 2158–2160 (2000).
6. O. Zhuromskyy, H. Dötsch, M. Lohmeyer, L. Wilkens, and P. Hertel, "Magnetooptical waveguide with polarization-independent nonreciprocal phaseshift," J. Lightwave Technol. **19**, 214–221 (2001).
7. H. Yokoi, T. Mizumoto, N. S. N. Futakuchi, and Y. Nakano, "Demonstration of an optical isolator with a semiconductor guiding layer that was obtained by use of a nonreciprocal phase shift," Appl. Opt. **39**, 6158–6164 (2000).
8. T. Shintaku, "Integrated optical isolator based on efficient nonreciprocal radiation mode conversion," Appl. Phys. Lett. **73**, 1946–1948 (1998).
9. T. Izuhara, J. Fujita, M. Levy, and R. M. Osgood, Jr., "Integration of magnetooptical waveguides onto a III–V semiconductor surface," IEEE Photonics Technol. Lett. **14**, 167–169 (2002).
10. H. Yokoi, T. Mizumoto, M. Shimizu, T. Waniishi, N. Futakuchi, N. Kaida, and Y. Nakano, "Analysis of GaInAsP surfaces by contact-angle measurement for wafer direct bonding of garnet crystals," Jpn. J. Appl. Phys. **38**, 4780–4783 (1999).
11. M. Takenaka and Y. Nakano, "Proposal of a novel semiconductor optical waveguide isolator," presented at the 11th International Conference on Indium Phosphide and Related Materials, Davos, Switzerland, May 16–20, 1999.
12. W. Zaets and K. Ando, "Optical waveguide isolator based on nonreciprocal loss/gain amplifier covered by ferromagnetic layer," IEEE Photonics Technol. Lett. **11**, 1012–1014 (1999).
13. A. K. Zvezdin and V. A. Kotov, *Modern Magnetooptics and Magnetooptical Materials* (Institute of Physics Publishing, Bristol, UK, 1997).
14. L. Wilkens, D. Träger, H. Dötsch, A. F. Popkov, and A. M. Alekseev, "Nonreciprocal phase shift of TE modes induced by a compensation wall in a magneto-optic rib waveguide," Appl. Phys. Lett. **79**, 4292–4294 (2001).
15. T. Mizumoto, Department of Electrical and Electronic Engineering, Tokyo Institute of Technology, Tokyo (personal communication, 2004).
16. H. Shimizu and M. Tanaka, "Design of semiconductor-waveguide-type optical isolators using the nonreciprocal loss/gain in the magneto-optical waveguides having MnAs nanoclusters," Appl. Phys. Lett. **81**, 5246–5248 (2002).
17. M. Vanwolleghem, W. Van Parys, S. Verstuyft, R. Wirix-Speetjens, L. Lagae, J. De Boeck, and R. Baets, "Ferromagnetic-metal-based InGaAs(P)/InP optical waveguide isolator: electrical and magneto-optical characterization," in *Proceedings of The Annual Symposium of the IEEE/LEOS Benelux Chapter* (Institute of Electrical and Electronics Engineers, Piscataway, N.J., 2002), pp. 282–285.
18. E. P. O'Reilly and A. R. Adams, "Band-structure engineering in strained semiconductor lasers," IEEE J. Quantum Electron. **30**, 366–379 (1994).
19. J. Decobert, N. Lagay, C. Cuisin, and B. Dagens, "MOVPE growth of AlGaInAsInP highly tensile-strained MQW's for 1.3 μm low-threshold lasers," presented at the Twelfth International Conference on Metal Organic Vapor Phase Epitaxy, Maui, Hawaii, May 30–June 4, 2004.
20. M. Vanwolleghem, W. Van Parys, D. Van Thourhout, R. Baets, F. Lelarge, O. Gauthier-Lafaye, B. Thedrez, R. Wirix-Speetjens, and J. De Boeck, "Experimental verification of a novel integrated isolator concept," presented at the 29th European Conference on Optical Communication, Rimini, Italy, September 21–25, 2003.
21. M. Vanwolleghem, W. Van Parys, D. Van Thourhout, R. Baets, F. Lelarge, O. Gauthier-Lafaye, B. Thedrez, R. Wirix-Speetjens, and J. De Boeck, "First experimental demonstration of a monolithically integrated InP-based waveguide isolator," in *Optical Fiber Communication Conference*, Vols. 95/A and 95/B of the OSA Trends in Optics and Photonics Series (Optical Society of America, Washington, D.C., 2004), paper TuE6.
22. A. Yariv and P. Yeh, *Optical Waves in Crystals* (Wiley, London, 1984).

23. Š. Višňovský, "Magneto-optical ellipsometry," Czech. J. Phys., Sect. B **36**, 625–650 (1986).
24. D. W. Berreman, "Optics in stratified and anisotropic media: 4 × 4-matrix formulation," J. Opt. Soc. Am. **62**, 502–510 (1972).
25. P. Yeh, "Optics of anisotropic layered media: a new 4 × 4 matrix algebra," Surf. Sci. **96**, 41–53 (1980).
26. M. Mansuripur, "Analysis of multilayer thin-film structures containing magneto-optic and anisotropic media at oblique incidence using 2 × 2 matrices," J. Appl. Phys. **67**, 6466–6475 (1990).
27. K. Postava, T. Yamaguchi, and R. Kantor, "Matrix description of coherent and incoherent light reflection and transmission by anisotropic multilayer structures," Appl. Opt. **41**, 2521–2531 (2002).
28. Š. Višňovský, "Optics of magnetic multilayers," Czech. J. Phys., Sect. B **41**, 663–694 (1991).
29. K. Postava, J. Pištora, and Š. Višňovský, "Magneto-optical effects in ultrathin structures at transversal magnetization," Czech. J. Phys., Sect. B **49**, 1185–1204 (1999).
30. F. Abeles, "Recherches sur la propagation des ondes electromagnetiques sinusoidales dans les milieux stratifies: application aux couches minces," Ann. Phys. **5**, 596–640 (1950).
31. J. Lafait, T. Yamaguchi, J. M. Frigerio, A. Bichri, and K. Driss-Khodja, "Effective medium equivalent to a symmetric multilayer at oblique incidence," Appl. Opt. **29**, 2460–2465 (1990).
32. Š. Višňovský, "Magneto-optical permittivity tensor in crystals," Czech. J. Phys., Sect. B **36**, 1424–1433 (1986).
33. J. Pištora, K. Postava, and R. Šebesta, "Optical guided modes in sandwiches with ultrathin metallic films," J. Magn. Magn. Mater. **198–199**, 683–685 (1999).
34. W. H. Press, S. A. Teukolsky, W. T. Vetterling, and B. P. Flannery, *Numerical Recipes in C++: The Art of Scientifique Computing*, 2nd ed. (Cambridge U. Press, Cambridge, 2002).
35. T. D. Visser, H. Blok, B. Demeulenaere, and D. Lenstra, "Confinement factors and gain in optical amplifiers," IEEE J. Quantum Electron. **33**, 1763–1766 (1997).
36. A. F. Popkov, M. Fehndrich, M. Lohmeyer, and H. Dötsch, "Nonreciprocal TE-mode phase shift by domain walls in magnetooptic rib waveguides," Appl. Phys. Lett. **72**, 2508–2510 (1998).
37. C. Vassallo, *Optical Waveguide Concepts* (Elsevier, Amsterdam, 1991).
38. F. Olyslager, *Electromagnetic Waveguides and Transmission Lines* (Clarendon, Oxford, 1999).
39. O. J. Glembocki and H. Piller, "Indium phospide (InP)," in *Handbook of Optical Constants of Solids*, E. D. Palik, ed. (Academic, San Diego, Calif., 1985), pp. 503–516.
40. B. Jensen, in *Handbook of Optical Constants of Solids II*, E. D. Palik, ed. (Academic, San Diego, Calif., 1991), Chap. 6. Calculation of the refractive index of compound semiconductors below the band gap, pp. 125–149.
41. M. Muñoz, T. M. Holden, F. H. Pollak, M. Kahn, D. Ritter, L. Kronik, and G. M. Cohen, "Optical constants of $In_{0.53}Ga_{0.47}As/InP$: experiment and modeling," J. Appl. Phys. **92**, 5878–5885 (2002).
42. M. Compin, B. Bartenlian, P. Beauvillain, P. Gogol, J. Hamrle, L. Lagae, J. Pistora, K. Postava, S. Visnovsky, and R. Wirix-Speetjens, "Détermination des indices optiques et magnéto-optiques de films minces de CoFe constituant un isolateur intégré à 1.3 μm," presented at the Colloque Louis Neél CMNM 2004, Autrans, France, March 17–19, 2004.
43. K. Postava, J. Pištora, and T. Yamaguchi, "Magneto-optic vector magnetometry for sensor applications," Sens. Actuators, A **110**, 242–246 (2004).